Amorphous TiO_2-Au thin film composites synthesized by pulsed laser deposition

L. Meza-León, A. Chávez-Chávez, J.G. Quiñones-Galván

TiO_2 has been widely studied and synthesized by various methods due to its excellent optoelectronic properties. It is possible to modify the optical properties of TiO_2 by incorporating noble metal nanoparticles in order to improve its photoresponse. In this work, TiO_2-Au thin film composites were grown by pulsed laser deposition technique. Ti and Au targets were simultaneously ablated in order to produce combined plasmas under a reactive atmosphere containing oxygen at a pressure of 2×10^{-2} Torr. The plasmas were analyzed individually by means of a planar Langmuir probe in order to calculate their mean kinetic ion energy and plasma density. Ti plasma parameters were kept constant at 196 eV and 2.06×10^{13} cm^{-3} while the Au plasma density was varied from 2.65×10^{12} cm^{-3} to 22.4×10^{12} cm^{-3}. The samples were characterized by UV-Vis spectroscopy and scanning electron microscopy. The band gap of the films was determined by means of the Tauc method, which decreased from 2.36 to 1.54 eV as the Au plasma density increased. The resultant morphology of the films shows the formation of spherical Au nanoparticles, whose average sizes increases as the Au plasma density increased, resulting in values ranging from 15 to 72 nm.

Introduction

In the field of photocatalysis, TiO_2 has been the most widely studied material due to its chemical stability, non-toxicity, low cost and long durability. However, since this material has a large band gap (3.2 eV), its photocatalytic activity is limited to ultraviolet radiation. Therefore, it is important to enhance the photocatalytic activity of TiO_2 toward visible region to maximize solar energy utilization. Various ways of modifying TiO_2 for its activation in the visible range of the spectrum have been studied, such as doping with metal ions [1], and non-metal ions [2], coupling with other semiconductors [3], deposition of metal nanoparticles [4] and sensitization using dyes [5]; in this way, it is possible to prevent recombination of the electron/hole pairs, reduce the band gap energy and increase light absorption range.

The most frequently used modification method is the preparation of composites by loading metal nanoparticles into a TiO_2 matrix. These nanoparticles significantly affect the photochemical properties of TiO_2 [6]. Particularly, the employment of noble metal nanoparticles (Ag, Au, Pt, Pd, Ru, etc.) is important since these nanoparticles can absorb visible light via surface plasmon resonance (SPR) in order to enhance photocatalytic activity [7,8]. There are various synthesis methods for preparation of noble metal nanoparticles-TiO_2 composites, such as ion exchange [9], hydrothermal [10], impregnation [11], photodeposition [12], among others. However, in comparison with the above-mentioned methods, thin film synthesis shows various advantages such as low production cost due to the reduction in material usage, miniaturization of the device, and easy material recovery. Some of the techniques used in thin films synthesis are by spray pyrolysis [13], sol-gel [14], pulsed laser deposition (PLD) [15], and thermal evaporation [16]. PLD has shown to be a promising technique in thin film synthesis due to various reasons, for instance, it provides precise stoichiometry transfer from target to film [17], it allows the ablation of a specific area, and the obtained films have high crystallinity. In addition, it is possible to modify the plasma parameters in order to control the composition of the thin films, and thus, its properties [18]. In this work, TiO_2-Au thin films were prepared by PLD technique by the simultaneous laser ablation of Ti and Au targets under a reactive oxygen atmosphere in order to study the effect of Au content in the thin film properties by varying the Au plasma density, while Ti plasma parameters were kept constant.

Experimental details

TiO_2-Au thin films were grown on quartz substrates by pulsed laser ablation technique. High purity Ti and Au targets with 5 and 2.5 cm in diameter, were coaxially attached in order to be simultaneously ablated (Figure 1). The Ti and Au targets were placed at 5 and 4.8 cm from the substrate. The depositions were carried out inisde a vacuum chamber evacuated to a base pressure of 4×10^{-6} Torr. As a reactive atmosphere, a gas mixture of 20% O_2 and 80% Ar was used at a deposition pressure of 2×10^{-2} Torr.

For the ablation process, a Quantel (Brilliant B) Nd:YAG laser emitting at a wavelength of 1064 nm, repetition rate of 10 Hz, output energy of 750 mJ per pulse, and a pulse duration of 6 ns, was used. The targets were rotated at 15 rpm in order to avoid drilling during this process. The deposition time was 20 min for all experiments.

Titanium and gold plasmas were individually analyzed by Langmuir probe measurements. Their mean kinetic ion energy (E_k) and plasma density (N_p) were determined by the time of flight curves (TOF), which were obtained by a 6 mm diameter planar Langmuir probe biased at -44 V and placed at the position of the substrate. The voltage drop, across a 22 Ω resistor was recorded on a Tektronix 500 MHz digital oscilloscope in order to obtain the probe current. For the calculation of mean kinetic energy, the procedure described

Lilibeth Meza-León, A. Chávez-Chávez, J.G. Quiñones-Galván ✉
Departamento de Física, CUCEI, Universidad de Guadalajara, Guadalajara, Jalisco, 44430 México.

Received: September 27th, 2022
Accepted: September 15th, 2023
Published: October 4th, 2023

https://doi.org/10.47566/2023_syv36_1-230902

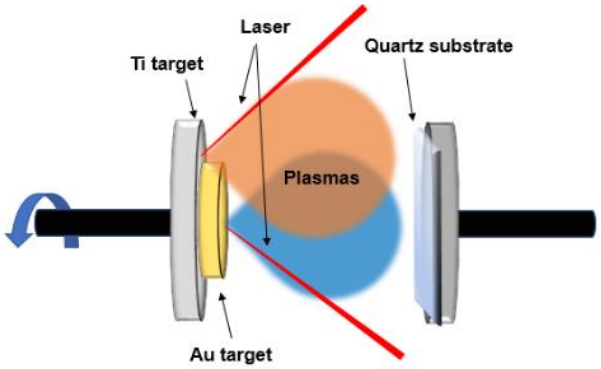

Figure 1. Schematic of the PLD setup.

in reference [19] was used, according to the following relationship:

$$\langle E_k \rangle = \frac{mL^2}{2} \frac{\int_0^T t^{-2} I(t) dt}{\int_0^T I(t) dt} \quad (1)$$

where m is the mass of the ion, L is the distance between the target and the probe, and I(t) is the probe current as a function of time.

The plasma density was calculated according to the following equation, described in reference [20]:

$$N_p = \frac{I_{max}}{e\upsilon A} \quad (2)$$

where I_{max} is the maximum value of the current of the TOF curves, e is the electron charge, υ is the plasma flow velocity, and A is the collecting area of the probe.

Thin films were grown by combining Ti and Au plasmas, keeping the laser fluence on the Ti target constant at 2.15 J/cm^2, while for the Au target, the laser fluence was varied using attenuators in order to modify the plasma properties and thereby change the Au content in each film.

The thickness of the films was determined by means of profilometry, using a KLA Tencor D-120 equipment. The optical absorbance and transmittance spectra of the thin films were obtained using a Thermo Scientific (Genesys 10) UV-Vis spectrophotometer from 200 to 1100 nm. The morphology of the films was observed by scanning electron microscopy using a Tescan (MIRA 3) field emission scanning electron microscope (FESEM) at 15 kV. The ImageJ software was employed to analyze the obtained SEM images.

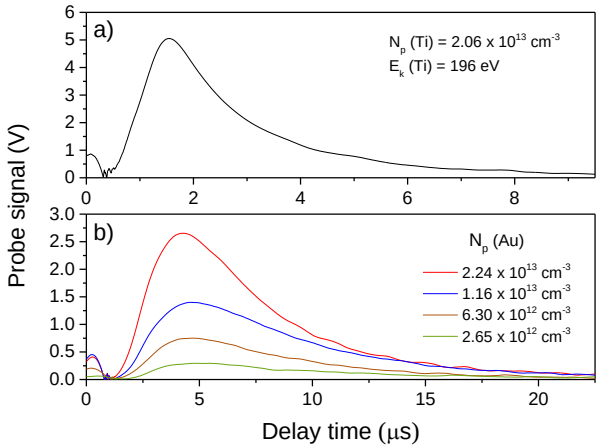

Figure 2. Time of flight curves of a) Ti and b) Au plasmas.

Results and discussion

TOF curves of Ti and Au plasmas are shown in Figure 2, from which the mean kinetic energy and plasma density were obtained using the equations 1 and 2.

One TiO_2 film was deposited as a reference, while four others were deposited with different Au plasma densities. Therefore, the plasma parameters were kept constant for the Ti target, at 196 eV and 2.06×10^{13} cm^{-3} for all the deposits. For the Au plasma, the plasma density was varied with the help of attenuators such that the mean kinetic energy kept constant for all experiments. The mean kinetic energy was 89 eV approximately. Regarding the plasma density, it was varied from 2.65×10^{12} cm^{-3} to 22.4×10^{12} cm^{-3}. As it can be seen in Figure 2b, since plasma density depends on the maximum current value of the TOF curve, therefore, when the height in the TOF curves changes, this will produce a change in plasma density as well [18].

In order to analyze the optical properties of the thin films, the absorbance and transmittance spectra were obtained with the help of the UV-Vis spectrophotometer. Figure 3a shows the absorbance spectra of the films. For the samples TiO_2-Au, the appearance of absorption bands at 590, 596, 642, and 650 nm, for increasing Au plasma density can be observed, which are attributed to the surface plasmon resonance (SPR) of Au incorporated in the TiO_2 matrix, indicating absorption in the visible range of the spectrum and the presence of

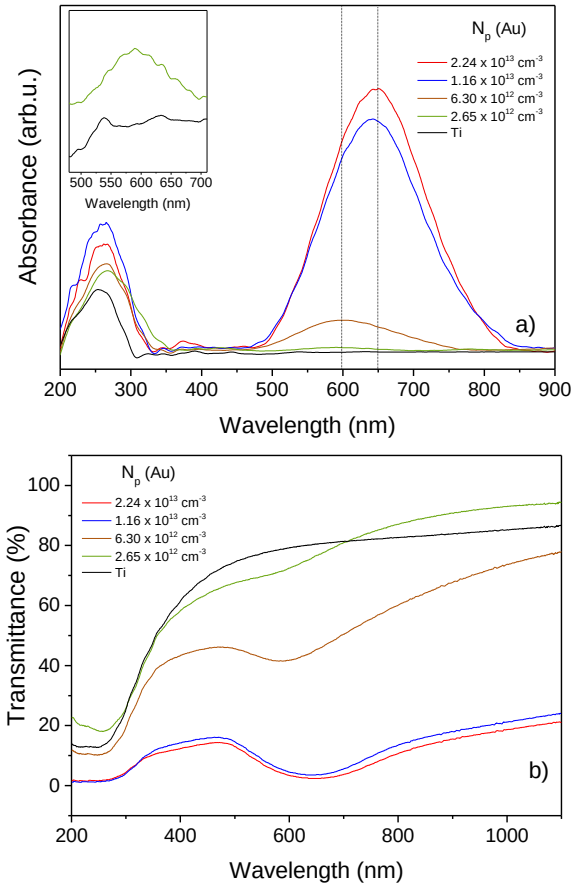

Figure 3. a) Absorbance and b) transmittance spectra for TiO_2 and TiO_2-Au thin films

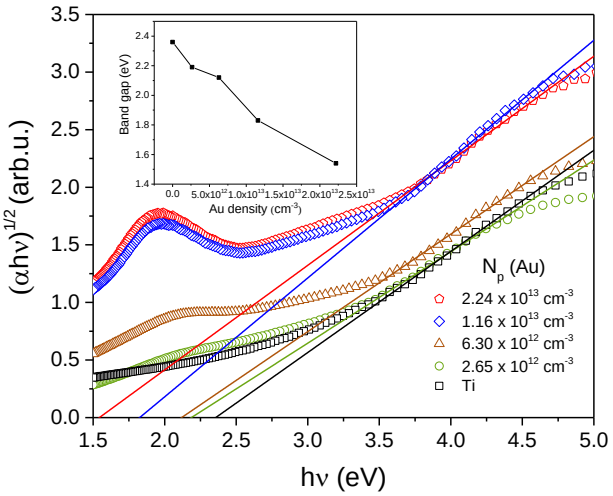

Figure 4. Tauc plots of TiO_2 and TiO_2-Au thin films. The inset displays the band gap dependence on Au plasma density.

spherical particles of nanometric size. A redshift of the peak positions can be observed, indicating that the nanoparticles size increases [21]. In addition, it is observed that the absorbance of the thin films increases for higher densities of the Au plasma density. A significant difference between the plasmon resonance bands of the brown and blue lines in the graph of Figure 3 can be noticed. This difference is attributed to the increase in Au ion density, with the brown graph having a density of 6.30×10^{12} cm^{-3} and the blue graph having a density of 11.6×10^{12} cm^{-3}, resulting in an increase in the Au nanoparticles content incorporated into the films. Furthermore, an increment of film thickness occurs on all the samples, due to the higher Au ion density and the consequent increment of Au content into the films, allowing an increase of 50 nm of the sample without Au incorporated, to ~100 nm for the film grown with the highest Au ion density. Hence, the amplitude of the surface plasmon resonance peaks increases with the increase of film thickness [22]. It is worth mentioning that only measurements of the thickness of these two films were obtained. Therefore, the thickness of the other films should lie between the two mentioned values, according to previously reported observations [23,24].

The latter result indicates that there is not a lineal relationship between Au plasma density and the amplitude of the SPR absorption band. The increase in amplitude for increasing density from 2.65 to 6.30×10^{12} cm^{-3} and from 11.6 to 22.4×10^{12} cm^{-3} is not as noticeable as the increase from 6.30 to 11.6×10^{12} cm^{-3}. At lower Au plasma density values, the SPR absorption band amplitude is low, meaning that small quantities of gold coalesce to form embedded nanoparticles within the TiO_2 matrix. However, when the Au ions reaching the substrate surface is increased to 11.6×10^{12} cm^{-3}, the quantity of Au nanoparticles is drastically increased, as revealed by the high amplitude of the SPR band, nevertheless, further increase in Au density, does not induce a significant increase in Au nanoparticles incorporated into the matrix. We may assume that the increasing scattering processes together with re-sputtering from arriving species to the surfaces in the combined plasmas, prevent formation of higher quantity of nanoparticles.

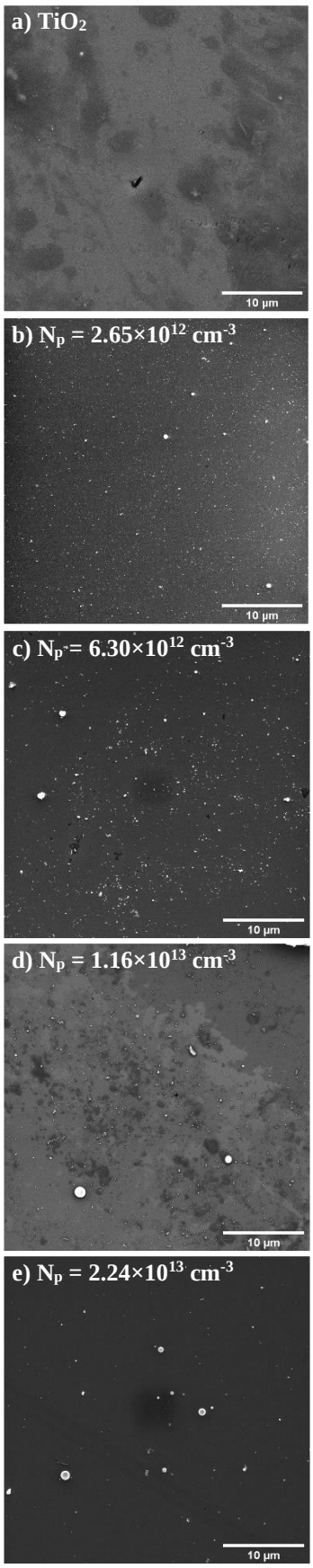

Figure 5. Scanning electron microscopy (SEM) images of TiO_2 and TiO_2-Au thin films.

Table 1. Au nanoparticles average size for the TiO_2-Au thin films.

Au plasma density (cm^{-3})	Average size (nm)
2.65×10^{12}	15
6.30×10^{12}	21
1.16×10^{13}	34
2.24×10^{13}	72

Figure 3b shows the transmittance spectra of the films. It can be seen that when Au nanoparticles are incorporated, the transmittance decreases, which indicates higher absorption in the visible range of spectrum [25].

The band gap (E_g) was determined from UV-Vis measurements using the Tauc method. Figure 4 shows the Tauc plots, where $(\alpha h\nu)^{½}$ vs $h\nu$ was plotted. Therefore, applying an extrapolation of the linear region of the curves to the abscissa $(\alpha h\nu)^{½} = 0$, the E_g values were obtained. The E_g value for the amorphous TiO_2 thin film was 2.36 eV, while for the TiO_2-Au thin films were 2.19, 2.12, 1.83, and 1.54 eV, respectively. The dependence of the band gap of the samples on the Au plasma density can be noticed (inset in Figure 4). It is observed that the band gap decreases as the Au plasma density on the films increases.

Figure 5 shows the SEM images, which were obtained at 5000 times magnification. Figure 5a corresponds to amorphous TiO_2 thin film. It can be seen that its surface is smooth and uniform. Figure 5b-5e correspond to the Au incorporated into the films. It can be noticed the formation of spherical particles of nanometric size. Each film was analyzed by ImageJ software, where the extraction of the cross-sectional area A for individual particles was obtained. Then, nanoparticle sizes were estimated by using the formula $d = 2(A/\pi)^{½}$, and their average was computed. Table 1 shows the average sizes of Au nanoparticles for each of the films.

As it can be noticed, the size of the nanoparticles increases with increasing the Au plasma density, thus nanoparticles with an average size in the range of 15-72 nm were obtained. These results are in agreement with those observed in UV-Vis measurements.

Conclusions

TiO_2-Au thin film composites with different Au content were obtained by PLD technique by combining Ti and Au plasmas in a reactive oxygen atmosphere. It was possible to control Au content incorporated into the films by manipulating Au plasma parameters. It was shown that the properties of the films were heavily dependent on the Au plasma density. The band gap of the films was reduced from 2.19 to 1.54 eV as the Au content was increased. SEM images showed formation of spherical nanoparticles, which average sizes increased with increasing Au plasma density, ranging from 15 to 72 nm. This shows the importance of plasma diagnosis in the PLD technique, owing that we can have control of the properties of the films and have reproducibility in the experiments.

Acknowledgements

The authors thank the technical support of Sergio Oliva. L.J.M.L. acknowledges CONACyT for her master's degree scholarship.

References

[1]. D. Jiang, T.A. Otitoju, Y. Ouyang, N.F. Shoparwe, S. Wang, A. Zhang, S. Li, *Catalysts* **11**, 1039 (2021).
[2]. A. Mittal, B. Mari, S. Sharma, V. Kumari, S. Maken, K. Kumari, N. Kumar, *J Mater Sci: Mater Electron.* **30**, 3186 (2019).
[3]. H.M. Mousa, J.F. Alenezi, I.M.A. Mohamed, A.S. Yasin, A.-F.M. Hashem, A. Abdal-hay, *J. Alloys Compd.* **886**, 161169 (2021).
[4]. X. Yang, Y. Wang, L. Zhang, H. Fu, P. He, D. Han, T. Lawson, X. An, *Catalysts* **10**, 139 (2020).
[5]. X. Li, J.-L. Shi, H. Hao, X. Lang, *Appl. Catal. B: Environ.* **232**, 260 (2018).
[6]. H. Park, Y. Park, W. Kim, W. Choi, *J. Photochem. Photobiol. C: Photochem. Rev.* **15**, 1 (2013).
[7]. X. Zhou, G. Liu, J. Yu, W. Fan, *J. Mater. Chem.* **22**, 21337 (2012).
[8]. A. Kumar, P. Choudhary, A. Kumar, P.H.C. Camargo, V. Krishnan, *Small* **18**, 2101638 (2022).
[9]. Q. Yang, M. Hu, J. Guo, Z. Ge, J. Feng, *J. Materiomics* **4**, 402 (2018).
[10]. J. Yu, L. Yue, S. Liu, B. Huang, X. Zhang, *J. Colloid Interface Sci.* **334**, 58 (2009).
[11]. G.G. Lenzi, C.V.B. Fávero, L.M.S. Colpini, H. Bernabe, M.L. Baesso, S. Specchia, O.A.A. Santos, *Desalination* **270**, 241 (2011).
[12]. S.C. Chan, M.A. Barteau, *Langmuir* **21**, 5588 (2005).
[13]. M.O. Abou-Helal, W.T. Seeber, *Appl. Surf. Sci.* **195**, 53 (2002).
[14]. R.S. Sonawane, M.K. Dongare, *J. Mol. Catal. A: Chem.* **243**, 68 (2006).
[15]. L. Meng, Z. Wang, L. Yang, W. Ren, W. Liu, Z. Zhang, T. Yang, M.P. dos Santos, *Appl. Surf. Sci.* **474**, 211 (2019).
[16]. L. Bedikyan, S. Zakhariev, M. Zakharieva, *J. Chem. Technol. Metall.* **48**, 555 (2013).
[17]. J. Schou, *Appl. Surf. Sci.* **255**, 5191 (2009).
[18]. S. Saracho-González, A. Pérez-Centeno, M.A. Santana-Aranda, G. Gómez-Rosas, A. Chávez-Chávez, E. Camps, L.P. Rivera, F. de Moure-Flores, O. Zelaya-Angel, J.G. Quiñones-Galván, *Mater. Sci. Semicond. Process.* **87**, 7 (2018).
[19]. N.M. Bulgakova, A.V. Bulgakov, O.F. Bobrenok, *Phys. Rev. E* **62**, 5624 (2000).
[20]. B. Doggett, J.G. Lunney, *J. Appl. Phys.* **105**, 033306 (2009).
[21]. M. Ghidelli, L. Mascaretti, B.R. Bricchi, A. Brognara, T.A. Afifi, V. Russo, C.S. Casari, A.L. Bassi, *Semicond. Sci. Technol.* **35**, 035016 (2020).
[22]. V.N. Rai, A.K. Srivastava, *JSM Nanotechnol. Nanomed.* **4**, 1039 (2016).
[23]. J.G. Quiñones-Galván, D. Cardona, L.P. Rivera, G. Gómez-Rosas, A. Chávez-Chávez, *Mater. Lett.* **284**, 129024 (2021).
[24]. J.A. Guerrero de León, A. Pérez-Centeno, G. Gómez-Rosas, E. Camps, J.S. Arias-Cerón, M.A. Santana-Aranda, J.G. Quiñones-Galvan, *Mater. Res. Express* **7**, 016423 (2020).
[25]. L.A. Martínez-Chávez, E.M. Rivera-Muñoz, R.R. Velázquez-Castillo, L. Escobar-Alarcón, K. Esquivel, *Catalysts* **11**, 1406 (2021).